

Circuit quantum electrodynamics with a quadruple quantum dot

Ting Lin(林霆), Hai-Ou Li(李海欧), Gang Cao(曹刚), and Guo-Ping Guo(郭国平)

Citation: Chin. Phys. B, 2023, 32 (**7**): 070307. DOI: 10.1088/1674-1056/accd57
Journal homepage: http://cpb.iphy.ac.cn; http://iopscience.iop.org/cpb

What follows is a list of articles you may be interested in

Change-over switch for quantum states transfer with topological channels in a circuit-QED lattice

Liu-Yong Cheng(程留永), Li-Na Zheng(郑黎娜), Ruixiang Wu(吴瑞祥), Hong-Fu Wang(王洪福), and Shou Zhang(张寿)

Chin. Phys. B, 2022, 31 (**2**): 020305. DOI: 10.1088/1674-1056/ac2f2e

Dissipative generation for steady-state entanglement of two transmons in circuit QED

Shuang He(何爽), Dan Liu(刘丹), Ming-Hao Li(李明浩)

Chin. Phys. B, 2019, 28 (**8**): 080303. DOI: 10.1088/1674-1056/28/8/080303

Spin manipulation in semiconductor quantum dots qubit

Ke Wang(王柯), Hai-Ou Li(李海欧), Ming Xiao(肖明), Gang Cao(曹刚), Guo-Ping Guo(郭国平)

Chin. Phys. B, 2018, 27 (**9**): 090308. DOI: 10.1088/1674-1056/27/9/090308

Entangled-photons generation with quantum dots

Yuan Li(李远), Fei Ding(丁飞), Oliver G Schmidt

Chin. Phys. B, 2018, 27 (**2**): 020307. DOI: 10.1088/1674-1056/27/2/020307

Qubits based on semiconductor quantum dots

Xin Zhang(张鑫), Hai-Ou Li(李海欧), Ke Wang(王柯), Gang Cao(曹刚), Ming Xiao(肖明), Guo-Ping Guo(郭国平)

Chin. Phys. B, 2018, 27 (**2**): 020305. DOI: 10.1088/1674-1056/27/2/020305

RAPID COMMUNICATION

Circuit quantum electrodynamics with a quadruple quantum dot

Ting Lin(林霆)[1,2], Hai-Ou Li(李海欧)[1,2], Gang Cao(曹刚)[1,2,†], and Guo-Ping Guo(郭国平)[1,2,3]

[1] *CAS Key Laboratory of Quantum Information, University of Science and Technology of China, Hefei* 230026, *China*
[2] *CAS Center for Excellence in Quantum Information and Quantum Physics, University of Science and Technology of China, Hefei* 230026, *China*
[3] *Origin Quantum Computing Company Limited, Hefei* 230088, *China*

(Received 14 February 2023; revised manuscript received 31 March 2023; accepted manuscript online 17 April 2023)

In this theoretical work, we describe a mechanism for the coupling between a plane structure consisting of four quantum dots and a resonator. We systematically study the dependence of the quadruple coupling strength and the qubit decoherence rate and point out the optimized operating position of the hybrid system. According to the transmission given by the input–output theory, the signatures in the resonator spectrum are predicted. Furthermore, based on the parameters already achieved in previous works, we prove that the device described in this paper can achieve the strong coupling limit, i.e., this approach can be used for system extension under the existing technical conditions. Our results show an effective and promotable approach to couple quantum dot structures in plane with the resonator and propose a meaningful extension method.

Keywords: semiconductor qubit, circuit quantum electrodynamics (QED), semiconductor quantum dot, scalable semiconductor-based circuit QED architectures

PACS: 73.21.La, 03.67.Lx, 42.50.Wk **DOI:** 10.1088/1674-1056/accd57

1. Introduction

Semiconductor qubits, encoded by the electron states isolated in quantum dots, are among the promising platforms for quantum computing processing.[1–5] To increase the number of qubits in semiconductor systems, there are a series of works focusing on the implementation of scalable architectures, including quantum dot arrays and crossbar networks.[6–8] Additionally, maturing circuit quantum electrodynamics (QED) architectures promise an alternative and effective approach in coupling nonlocal qubits and scaling up the number of qubits, whereby the microwave resonator serves as a quantum bus and provides photons as mobile carriers of quantum information.[9–13] Compared to superconducting qubits, semiconductor qubits can work in a strong magnetic field, and the hybrid circuit QED system promises an attractive platform for studying spin–light interactions.[14,15] Moreover, recent experimental progresses present that the semiconductor qubit has a potential high operation temperature of ~ 1 K.[16,17] Combined with the resonator with high superconducting critical temperature,[18,19] this achievement promises a circuit QED system that can work and perform quantum information processing at a higher temperature.

The first theoretical scheme for coupling quantum dots to the resonator was proposed in 2004, in which an electric charge in the double quantum dot (DQD) couples to photons stored in the resonator with dipole interaction.[20] Based on charge–photon coupling, some follow-up works put forward schemes to enable the coupling between spin qubits and a resonator via spin–charge hybridization.[21–24] Recently, benefitting from the application of high-impedance resonators, the coupling strength between semiconductor qubits and photons stored in the resonator has been greatly improved, leading to the achievement of the strong coupling limit in hybrid superconducting–semiconductor circuit QED systems[25–30] and demonstrating the potentiality in quantum information processing.[15,31–33] From these works, we can find an intuitive impression that the charge qubit has a large coupling strength and a poor coherence time, and the spin qubit is the opposite. Thus, how to balance the coupling strength and coherence time becomes an interesting and valuable question. To improve the charge qubit coherence time, some researchers propose a scheme to prevent the charge qubit from the charge noise on dipole axis by encoding a quadruple qubit.[34,35]

Although the expansion methods based on nearest-neighbor interaction (quantum dot networks) and long-range interaction (circuit QED architectures) have attracted significant interest, there is little research focusing on the combination of these two nonexclusive methods or showing the potential scheme of that. In this work, we propose an effective and promotable approach to couple quantum dot structures in plane with a resonator. The coupling mechanism between a resonator and four quantum dots from a honeycomb-like quantum dot network is systematically discussed. We predict the coupling strength and determine that the coupling of the encoded qubit to the resonator is based on quadrupole interaction. Since the dipole coupling between the qubit and the resonator is suppressed, the coherence time is prevented from the

[†]Corresponding author. E-mail: gcao@ustc.edu.cn

© 2023 Chinese Physical Society and IOP Publishing Ltd

charge noise. Then, we describe the decoherence processing in semiconductor quantum dot systems and provide a map of the dephasing rate as a function of quantum dot chemical potentials. Furthermore, we simulate the observable signatures of charge–photon coupling in the resonator spectrum, the vacuum Rabi splitting, and find the optimal working point for the coupling between the quadruple qubit and the resonator. Notably, the coupling mechanism can be used for quantum dot systems with more connections in the center dot.

2. Model

Referring to the device in Ref. [36], we give a device sketch. This approach can reduce electrostatic disorder and has inherent design flexibility for highly customizable device layouts. Figure 1(a) shows the sketch of the quadruple quantum dot (QQD), in which the center quantum dot (red) is capacitively coupled to three adjacent quantum dots (orange) and a resonator (not shown). Figure 1(b) shows the device consisting of a gate layer (gray) and a quantum dot layer (light blue) from top to bottom. In the gate layer, there are three kinds of gates (yellow), labeled with 'O', 'P', and 'T', for setting up and accumulating the quantum dots. Gates O is used for depleting carriers in a large area (pink region) and determining the region where the quantum dots can be set up. Gates P control the chemical potentials of quantum dots, and gates T control the interdot tunnel coupling. This structure can be a basic unit of a two-dimensional (honeycomb-like) quantum dot network, as shown in Fig. 1(c).

In our proposal, we consider a single electron shared among four quantum dots. We assume that three surrounding plunger gates are connected, and the chemical potentials of the left, the upper, and the right dots have the same value $\varepsilon_L = \varepsilon_U = \varepsilon_R = \varepsilon$. Meanwhile, the chemical potential of the center dot ε_C is tuned by an independent plunger gate. As for the electron tunneling between nearest-neighbor quantum dots, they are tuned into the same with amplitude t.

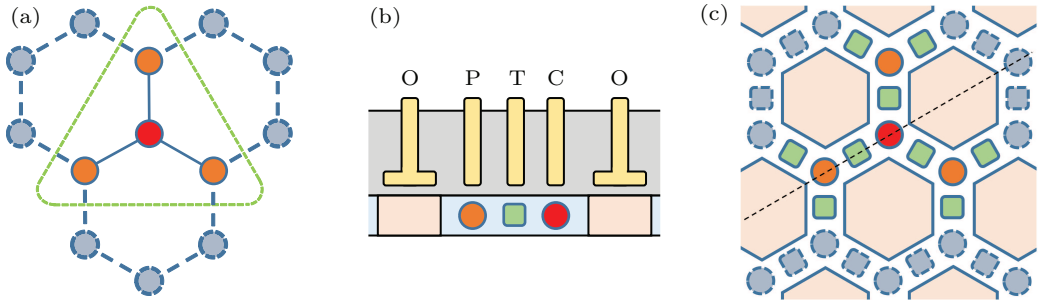


Fig. 1. Schematic illustration of the gate-defined QQD. (a) Simplified diagram of a QQD. (b) The cross-section of the device through the black dashed line in (c). (c) Top-down image of the quantum dot layer. In (a) and (c), the structure for future scaling is reserved and illustrated by the pattern marked by blue dotted lines.

3. Hamiltonian of the QQD

We now model the single electron QQD. According to the charge occupation, the electrons located on the center, the left, the upper, and the right quantum dots are denoted as states $|C\rangle$, $|L\rangle$, $|U\rangle$, and $|R\rangle$, respectively. On the basis of charge occupation, $\{|C\rangle, |L\rangle, |U\rangle, |R\rangle\}$, the QQD can be described by the Hamiltonian

$$H_{\mathrm{QQD}}/\hbar = \begin{pmatrix} E_C & -t & -t & -t \\ -t & 0 & 0 & 0 \\ -t & 0 & 0 & 0 \\ -t & 0 & 0 & 0 \end{pmatrix} + \varepsilon \mathbf{1}_4. \tag{1}$$

Here, $E_C = \varepsilon_C - \varepsilon$ is the center-dot detuning. Solving this Hamiltonian, we can obtain the eigenstates and their corresponding energy levels. The ordered energy levels are

$$E_0/\hbar = \varepsilon + \frac{1}{2}\left(E_C - \sqrt{E_C{+}12t^2}\right), \tag{2}$$

$$E_1/\hbar = \varepsilon, \tag{3}$$

$$E_2/\hbar = \varepsilon, \tag{4}$$

$$E_3/\hbar = \varepsilon + \frac{1}{2}(E_C + \sqrt{E_C{+}12t^2}). \tag{5}$$

Using the mixing angle ϕ, which satisfies equation $\sin\phi = \sqrt{12}t/\sqrt{E_C^2{+}12t^2}$, the corresponding eigenstates can be expressed as

$$|0\rangle = \cos(\phi/2)|S\rangle + \sin(\phi/2)|C\rangle, \tag{6}$$

$$|1\rangle = \frac{1}{\sqrt{2}}(|L\rangle - |R\rangle), \tag{7}$$

$$|2\rangle = \frac{1}{\sqrt{6}}(-|L\rangle + 2|U\rangle - |R\rangle), \tag{8}$$

$$|3\rangle = -\sin(\phi/2)|S\rangle + \cos(\phi/2)|C\rangle, \tag{9}$$

where $|S\rangle = \frac{1}{\sqrt{3}}(|L\rangle + |U\rangle + |R\rangle)$. These results are still effective when there exists a small difference among the chemical potentials of the left, the upper, and the right dot, i.e., $\left|\varepsilon_j - (\varepsilon_L + \varepsilon_U + \varepsilon_R)/3\right| \ll |\varepsilon_C|$, where $(j = L, U, R)$.

Figure 2 shows the eigenenergies of the four-level Hamiltonian as a function of E_C with a fixed detuning parameter $\varepsilon = 0$. While the energy levels of states $|0\rangle$ and $|3\rangle$ are tuned by varying E_C, states $|1\rangle$ and $|2\rangle$ are degenerate at energy $\hbar\varepsilon$. In our proposal, the quadruple qubit is encoded in states $|0\rangle$ and $|3\rangle$ with the qubit (operation) frequency

$$\omega_{\mathrm{a}} = \omega_{3,0} = (E_3 - E_0)/\hbar = \sqrt{E_C + 12t^2}. \tag{10}$$

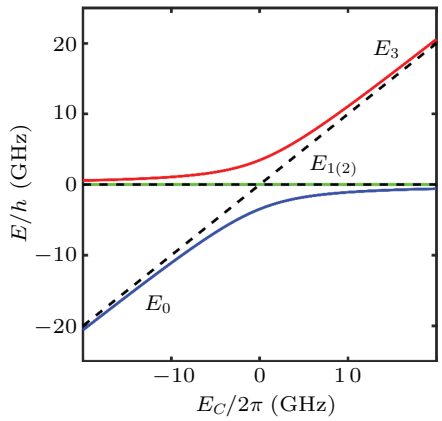


Fig. 2. Energy level E_n $(n = 0,\ldots,3)$ as a function of the center-dot detuning E_C. The dashed line is the energy level without interdot tunnel coupling ($t = 0$). Here, we calculate the energy levels with the parameters $\varepsilon = 0$ and $t/2\pi = 2$ GHz.

4. Coupling between a quadruple qubit and a resonator

The coupling between the QQD and a resonator is caused by the influence of the resonator electric field on the center dot chemical potentials and can be modeled as[20,34,37]

$$H_{\text{int}} = evV\left[\frac{3}{4}|C\rangle\langle C| - \frac{1}{4}\left(|L\rangle\langle L| + |U\rangle\langle U| + |R\rangle\langle R|\right)\right], \quad (11)$$

where e is the electron charge, v presents the conversion coefficient of resonator voltage applied to the center dot, and operator V presents the voltage on the resonator near the center dot. Since all resonator modes far detuned with the qubit are neglected, the coupling can be described as

$$\begin{aligned} H_{\text{int}} &= 2g_0(a+a^\dagger)\left[\frac{3}{4}|C\rangle\langle C|\right. \\ &\left. -\frac{1}{4}\left(|L\rangle\langle L| + |U\rangle\langle U| + |R\rangle\langle R|\right)\right]. \end{aligned} \quad (12)$$

Here, the annihilation operator a and creation operator $a^\dagger$ are for the relevant resonator mode with frequency ω_{r}. $g_0 = v\omega_{\text{r}}\sqrt{2Z_{\text{r}}/R_{\text{Q}}}$ is the overall coupling strength, Z_{r} is the resonator characteristic impedance, and $R_{\text{Q}} = h/e^2$ is the resistance quantum. According to recent experimental achievements using high-impedance resonator, the overall coupling strength g_0 can be around $2\pi\cdot 100$ MHz.[25,29,33] Furthermore, we write the interaction in the eigenbasis of the Hamiltonian shown in Eq. (1),

$$H_{\text{int}} = g_0(a+a^\dagger)\sum_{n,m=0}^{3} d_{n,m}|n\rangle\langle m|, \quad (13)$$

with the normalized photon coupling strength

$$\begin{aligned} d_{n,m} &= 2\langle n|\left[\frac{3}{4}|C\rangle\langle C|\right. \\ &\left. -\frac{1}{4}\left(|L\rangle\langle L| + |U\rangle\langle U| + |R\rangle\langle R|\right)\right]|m\rangle. \end{aligned} \quad (14)$$

Thus, we can obtain the photon coupling strength to the transition $0 \leftrightarrow 3$ as

$$g_{\text{q}} = g_0 d_{0,3} = g_0 d_{3,0} = g_0 \sin\phi. \quad (15)$$

We note that the qubit does not have a dipole moment, since $-e\langle 3|x|0\rangle$ is equal to zero, where x is the position operator. This indicates that the qubit can be protected from charge noise from the environment on the dipole axis.[34,35] As for the quadrupole moment, it can be determined as $-2e^2\langle 3|x^2|0\rangle \propto \sin\phi$. Thus, we can consider that the quadruple coupling plays a leading role in the charge–photon interaction, and the dipole coupling is suppressed.

In Fig. 3, we estimate the magnitude of the coupling, where g_{q}/g_0 is according to Eq. (15) and as a function of the center-dot detuning E_C and the interdot tunnel coupling t. When $E_C = 0$, as illustrated by the red dashed line, the coupling strength g_{q} reaches its maximum g_0. In the region where $|E_C| < t$, the ratio of g_{q} to g_0 exceeds 0.96. For the case that $|E_C|$ is much larger than t, states $|0\rangle$ and $|1\rangle$ are approximated by $|S\rangle$ and $|L\rangle$, respectively. Since the qubit has a small quadrupole moment $-2e^2\langle 3|x^2|0\rangle \sim -2e^2\langle L|x^2|S\rangle = 0$, the coupling between the quadruple qubit and the resonator becomes quite weak.

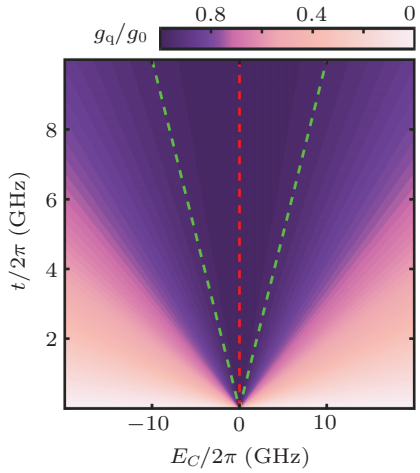


Fig. 3. Calculated coupling strength as a function of E_C and t. The red dashed line corresponds to $E_C = 0$, and the green dashed lines correspond to $E_C = \pm t$.

5. Decoherence rate of the quadruple qubit

In gate-defined quantum dot systems, the qubit decay is caused by the charge–phonon coupling and should be of the order of a few MHz.[38–40] The dephasing is caused by the charge noise, which originates from random charge fluctuations of material or the control and confinement voltage giving rise to fluctuation energies. And the decoherence rate is given by $\gamma = \frac{1}{2}\gamma^r + \gamma^\varphi$, where γ^r is the decay rate and γ^φ is the dephasing rate.

In this paper, we assume that all charge fluctuations satisfy Gaussian-distributed $1/f$ noise with a power spectral density $S_q(\omega) = A_q|\omega|^{-1}$, where $q \in \{\varepsilon_C, \varepsilon\}$ and $A_q = \sigma_q^2$ is the

variance of noise power spectral density. The dephasing rate for the quadruple qubit can be approximated by the analytical expression[34,41]

$$\gamma^{\varphi} = \gamma^{\varphi}_{3,0} = \frac{1}{\hbar}\left[\sum_{p}\left(\frac{1}{4}\omega_p^2 A_p + \frac{1}{16}\omega_{p,p}^2 A_p^2\right) + \sum_{p\neq q}\frac{1}{8}\omega_{p,q}^2 A_p A_q\right]^{\frac{1}{2}}, \tag{16}$$

where we use the definitions $\omega_p \equiv \partial\omega_{3,0}/\partial p$ and $\omega_{p,q}\equiv\partial^2\omega_{3,0}/\partial p\partial q$ with $p,q\in\{\varepsilon_C,\varepsilon\}$. For the case that the chemical potentials of the left, the upper, and the right dots are controlled by three independent plunger gates, we should consider about two additional detuning parameters in the dephasing processing, i.e., $p,q\in\{\varepsilon_C,\varepsilon_L,\varepsilon_U,\varepsilon_R\}$.

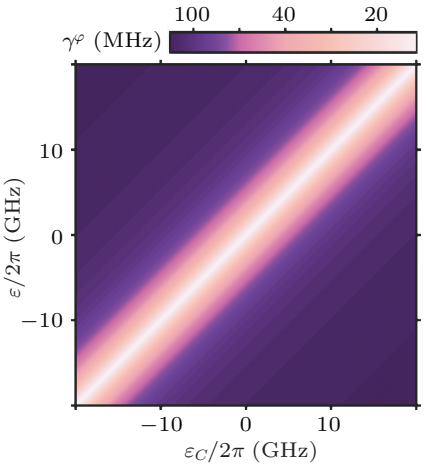


Fig. 4. Dephasing rate γ^{φ} as a function of ε_C and ε. We have chosen $A_{\varepsilon_C}/h^2 = 100^2$ MHz^2, $A_{\varepsilon}/h^2 = 200^2$ MHz^2, and $t/2\pi = 1.5$ GHz.

Figure 4 shows the calculated dephasing rate γ^{φ} as a function of the chemical potentials of the center dot ε_C and the detuning parameter ε. The calculated result is symmetrical about the diagonal ($\varepsilon_C = \varepsilon$). And we can find that the dephasing rate reaches its minimum at $\varepsilon_C = \varepsilon$, where the dephasing rate caused by the charge noise in first order $\frac{1}{4}\omega_p^2 A_p$ can be negligible.

6. Resonator spectrum

After determining the system parameters of a QQD coupling to a resonator, let us describe the response of the hybrid system in teh resonator spectrum. Here, we assume a probing microwave transmitting through the resonator with frequency $\omega_{\rm p}$ and the resonator decay rate $\kappa = \kappa_{\rm i} + \kappa_1 + \kappa_2$ consisting of the internal photon decay rate $\kappa_{\rm i}$ and the external photon decay rate through the input and output ports (κ_1 and κ_2). Within a rotating-wave approximation, we can obtain the transmission by employing input–output theory,[23,32]

$$S_{21} = \frac{-{\rm i}\sqrt{\kappa_1\kappa_2}}{\omega_{\rm r} - \omega_{\rm p} - {\rm i}\kappa/2 + g_0\sum\limits_{n=0}^{3}\sum\limits_{m=n+1}^{3} d_{n,m}\chi_{n,m}}, \tag{17}$$

where $\chi_{n,m} = \frac{-g_0 d_{m,n}(P_n - P_m)}{(E_m - E_n)/\hbar - \omega_{\rm p} - {\rm i}\gamma_{m,n}}$ is the electric susceptibilities of the electron charge state, P_n denotes the occupation probability of state $|n\rangle$, and $\gamma_{m,n}$ is the decoherence rate between states $|m\rangle$ and $|n\rangle$. Considering the case that the device works at the temperature $T \sim 0$ K, the QQD should be in its ground state, i.e., $P_n = \delta_{n,0}$. Thus, only the transitions $0 \leftrightarrow n$ ($n = 1,2,3$) should be discussed. Moreover, since the normalized photon coupling strength of transition $0 \leftrightarrow 1$ ($0 \leftrightarrow 2$) coupling to the resonator is equal to zero, the term of corresponding transitions $d_{n,m}\chi_{n,m}$ can be neglected. Based on the discussions above, Eq. (17) can be simplified as

$$S_{21} = \frac{-{\rm i}\sqrt{\kappa_1\kappa_2}}{\omega_{\rm r} - \omega_{\rm p} - {\rm i}\kappa/2 + g_0 d_{0,3}\chi_{0,3}}. \tag{18}$$

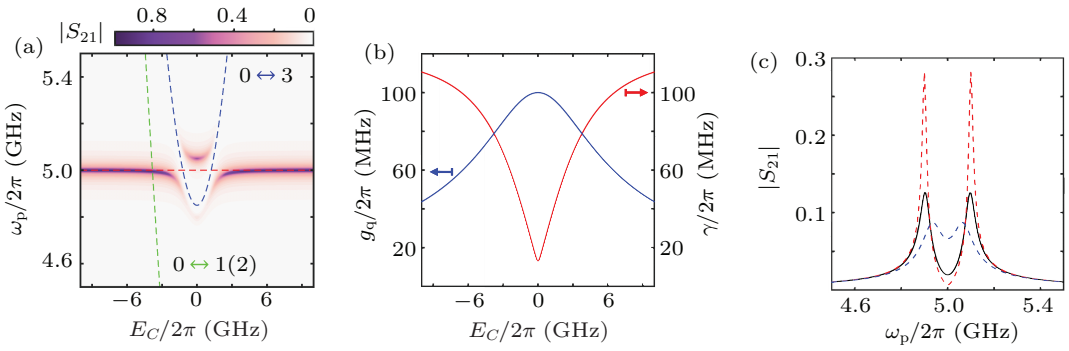


Fig. 5. (a) Resonator transmission spectrum $|S_{21}|$ as a function of E_C and $\omega_{\rm p}$. (b) The coupling strength $g_{\rm q}$ and the qubit decoherence rate γ used in (a) as a function of E_C. (c) Calculated vacuum Rabi splitting with $(E_C,t)/2\pi = (0, 1.44)$ GHz (red dashed line), $(E_C,t)/2\pi = (1.22, 1.40)$ GHz (black line), and $(E_C,t)/2\pi = (3.24, 1.10)$ GHz (blue dashed line). In these calculations, we have chosen $\kappa_1 = \kappa_2 = \kappa/2 = 2\pi\cdot 5$ MHz, $\omega_{\rm r}/2\pi = 5$ GHz, and the overall coupling strength $g_0/2\pi = 100$ MHz. The parameters about qubit decoherence processing are $\gamma^r = 20$ MHz, $A_{\varepsilon_C}/h^2 = 100^2$ MHz^2, and $A_{\varepsilon}/h^2 = 200^2$ MHz^2. The coherence parameters refer to Ref. [34].

In Fig. 5(a), we show the calculated transmission as a function of the center-dot detuning E_C and the probe frequency $\omega_{\rm p}$. Here, the amplitude of interdot tunnel coupling t is chosen as $t = 1.4$ GHz $< \omega_{\rm r}/\sqrt{12}$ to ensure the observation of vacuum Rabi splitting in the resonator spectrum. The blue (red) dashed line represents the frequency of the uncoupled quadruple qubit (resonator). As the qubit is tuned close to the resonator, the avoided crossing caused by the charge–photon

hybridization can be observed, i.e., the original spectral line of the resonator will split into two spectral lines in the transmission spectrum. When the quadruple qubit is in resonance with the resonator at $E_C = \pm\sqrt{\omega_r^2 - 12t^2}$ (the intersections of the blue and red dashed lines), the vacuum Rabi splitting of size $2g_q/2\pi$ can be observed. The green dashed line represents the transitions $0 \leftrightarrow 1$ and $0 \leftrightarrow 2$. Since these two transitions do not couple to the resonator, there is no corresponding avoided crossing in the resonator spectrum. If not, there must exist a difference among the chemical potentials of the left, the upper, and the right dot. Figure 5(b) shows the dependence of the coupling strength g_q and the qubit decoherence rate γ on the center-dot detuning E_C in Fig. 5(a). The coupling strength g_q reaches its maximum at $E_C = 0$, and the decoherence rate γ reaches its minimum at the same position. This result is general and can be derived from Eqs. (15) and (16). Thus, we can fix E_C at zero to improve the quantum coherence performance of the quadruple qubit. Figure 5(c) shows the calculated vacuum Rabi splitting with different E_C. As $|E_C|$ increases, two spectral lines become blurred and their distance decreases with decreasing g_q and increasing γ.

7. Discussion

According to the Eq. (15), the quadruple coupling strength can reach the overall coupling strength g_0 when $E_C = 0$. Thus, we can directly use the maximum charge-photon coupling strength $\max(g_d) = g_0$.[20] in the system with a DQD coupling to a resonator to estimate the quadruple coupling strength g_q. For the decoherence processing, if we set the working position at $E_C = 0$, the decoherence rate can reach its minimum. Since the dephasing rate of the quadruple qubit mainly caused by the charge noise in the first order is suppressed and equal to zero, the decoherence rate of the quadruple qubit should be not higher than the decoherence rate of a DQD charge qubit on the sweet spot.[42] Thus, we can directly estimate the performance of the quadruple qubit from a charge DQD qubit. Referring to the parameters shown in recent experiments, Refs. [25,32,33], our approach can already be realized in the strong coupling regime ($g > \gamma, \kappa$) and used for system extension under the existing technical conditions.

Also, the method mentioned in this work can be used in quantum dot systems with more connections in the center dot. For the case that the center dot coupling to N quantum dots, we can still encode the qubit in the lowest and the highest levels of the quantum dots system with frequency $\omega_a' = \sqrt{E_C^2 + 4Nt^2}$ and coupling strength $g_q' = g_0 \sin\phi' = \sqrt{2}Ntg_0/\omega_a'$.

8. Conclusion

In this paper, we describe how to couple an electron shared among four quantum dots to photons stored in a resonator. The general method for obtaining the coupling strength and the decoherence rate of transitions of the electron in the QQD is systematically discussed. We choose the lowest and the highest levels of the QQD to encode the quadruple qubit, which can prevent the qubit from charge noise on the dipole axis and avoid other transitions. After determining the coupling strength and the decoherence rate, we find the optimal working point for charge–photon coupling and obtain the resonator spectrum of the hybrid system using the transmission coefficient given by the input–output theory. In short, our results show that the coupling mechanism is effective and realistic for coupling the quantum dot structure in plane to a resonator, since the qubit coherence time is improved while maintaining the coupling strength. Also, our work indicates a potential application in connecting two extension methods based on quantum dot networks and hybrid circuit QED architectures.

Acknowledgement

Project supported by the National Natural Science Foundation of China (Grant Nos. 92265113, 12074368, and 12034018).

References

[1] Loss D and DiVincenzo D P 1998 *Phys. Rev. A* **57** 120
[2] Ladd T D, Jelezko F, Laflamme R, Nakamura Y, Monroe C and O'Brien J L 2010 *Nature* **464** 45
[3] Zwanenburg F A, Dzurak A S, Morello A, Simmons M Y, Hollenberg L C L, Klimeck G, Rogge S, Coppersmith S N and Eriksson M A 2013 *Rev. Mod. Phys.* **85** 961
[4] Zhang X, Li H O, Cao G, Xiao M, Guo G C and Guo G P 2019 *Natl. Sci. Rev.* **6** 32
[5] Chen Y, Lin F L, Liang X and Jiang N Q 2019 *Chin. Phys. Lett.* **36** 070302
[6] Fujita T, Baart T A, Reichl C, Wegscheider W and Vandersypen L M K 2017 *npj Quantum Inf.* **3** 22
[7] Li R, Petit L, Franke D P, Dehollain J P, Helsen J, Steudtner M, Thomas N K, Yoscovits Z R, Singh K J and Wehner S 2018 *Sci. Adv.* **4** eaar3960
[8] Mills A, Zajac D, Gullans M, Schupp F, Hazard T and Petta J 2019 *Nat. Commun.* **10** 1
[9] Majer J, Chow J M, Gambetta J M, Koch J, Johnson B R, Schreier J A, Frunzio L, Schuster D I, Houck A A and Wallraff A 2007 *Nature* **449** 443
[10] Sillanpää M A, Park J I and Simmonds R W 2007 *Nature* **449** 438
[11] Blais A, Gambetta J, Wallraff A, Schuster D I, Girvin S M, Devoret M H and Schoelkopf R J 2007 *Phys. Rev. A* **75** 032329
[12] Song C, Xu K, Liu W, Yang C P, Zheng S B, Deng H, Xie Q, Huang K, Guo Q and Zhang L 2017 *Phys. Rev. Lett.* **119** 180511
[13] Astner T, Nevlacsil S, Peterschofsky N, Angerer A, Rotter S, Putz S, Schmiedmayer J and Majer J 2017 *Phys. Rev. Lett.* **118** 140502
[14] Burkard G and Petta J R 2016 *Phys. Rev. B* **94** 195305
[15] Harvey-Collard P, Dijkema J, Zheng G, Sammak A, Scappucci G and Vandersypen L M 2022 *Phys. Rev. X* **12** 021026
[16] Petit L, Eenink H, Russ M, Lawrie W, Hendrickx N, Philips S, Clarke J, Vandersypen L and Veldhorst M 2020 *Nature* **580** 355
[17] Yang C H, Leon R, Hwang J, Saraiva A, Tanttu T, Huang W, Camirand Lemyre J, Chan K W, Tan K and Hudson F E 2020 *Nature* **580** 350
[18] Samkharadze N, Bruno A, Scarlino P, Zheng G, DiVincenzo D, DiCarlo L and Vandersypen L 2016 *Phys. Rev. Appl.* **5** 044004
[19] Wei X Y, Pan J Z, Lu Y P, Jiang J L, Li Z S, Lu S, Tu X C, Zhao Q Y, Jia X Q and Kang L 2020 *Chin. Phys. B* **29** 128401
[20] Childress L, Sørensen A S and Lukin M D 2004 *Phys. Rev. A* **69** 042302
[21] Hu X D, Liu Y X and Nori F 2012 *Phys. Rev. B* **86** 035314

[22] Srinivasa V, Taylor J M and Tahan C 2016 *Phys. Rev. B* **94** 205421

[23] Benito M, Mi X, Taylor J M, Petta J R and Burkard G 2017 *Phys. Rev. B* **96** 235434

[24] Benito M, Petta J R and Burkard G 2019 *Phys. Rev. B* **100** 081412

[25] Stockklauser A, Scarlino P, Koski J V, Gasparinetti S, Andersen C K, Reichl C, Wegscheider W, Ihn T, Ensslin K and Wallraff A 2017 *Phys. Rev. X* **7** 011030

[26] Mi X, Benito M, Putz S, Zajac D M, Taylor J M, Burkard G and Petta J R 2018 *Nature* **555** 599

[27] Samkharadze N, Zheng G, Kalhor N, Brousse D, Sammak A, Mendes U C, Blais A, Scappucci G and Vandersypen L M K 2018 *Science* **359** 1123

[28] Chen M B, Jiang S L, Wang N, Wang B C, Lin T, Gu S S, Li H O, Cao G and Guo G P 2021 *Phys. Rev. Appl.* **15** 044045

[29] Yu C X, Zihlmann S, Abadillo-Uriel J C, Michal V P, Rambal N, Niebojewski H, Bedecarrats T, Vinet M, Dumur E and Filippone M 2023 *Nat. Nanotechnol.* 1–6

[30] Lin T, Gu S S, Xu Y-Q, Jiang S L, Wang N, Wang B C, Li H O, Cao G and Guo G P 2022 *Appl. Phys. Lett.* **121** 184004)

[31] van Woerkom D J, Scarlino P, Ungerer J H, Müller C, Koski J V, Landig A J, Reichl C, Wegscheider W, Ihn T, Ensslin K and Wallraff A 2018 *Phys. Rev. X* **8** 041018

[32] Borjans F, Croot X G, Mi X, Gullans M J and Petta J R 2020 *Nature* **577** 195

[33] Wang B, Lin T, Li H, Gu S, Chen M, Guo G, Jiang H, Hu X, Cao G and Guo G 2021 *Science Bulletin* **66** 332

[34] Koski J V, Landig A J, Russ M, Abadillo-Uriel J C, Scarlino P, Kratochwil B, Reichl C, Wegscheider W, Burkard G and Friesen M 2020 *Nat. Phys.* **16** 642

[35] Friesen M, Ghosh J, Eriksson M and Coppersmith S 2017 *Nat. Commun.* **8** 15923

[36] Ha W, Ha S D, Choi M D, Tang Y, Schmitz A E, Levendorf M P, Lee K, Chappell J M, Adams T S and Hulbert D R 2021 *Nano Lett.* **22** 1443

[37] Landig A J, Koski J V, Scarlino P, Mendes U, Blais A, Reichl C, Wegscheider W, Wallraff A, Ensslin K and Ihn T 2018 *Nature* **560** 179

[38] Gasser U, Gustavsson S, Küng B, Ensslin K, Ihn T, Driscoll D and Gossard A 2009 *Phys. Rev. B* **79** 035303

[39] Mi X, Cady J V, Zajac D M, Deelman P W and Petta J R 2017 *Science* **355** 156

[40] Scarlino P, van Woerkom D J, Stockklauser A, Koski J V, Collodo M C, Gasparinetti S, Reichl C, Wegscheider W, Ihn T, Ensslin K and Wallraff A 2019 *Phys. Rev. Lett.* **122** 206802

[41] Russ M, Ginzel F and Burkard G 2016 *Phys. Rev.B* **94** 165411

[42] Abadillo-Uriel J, Eriksson M, Coppersmith S and Friesen M 2019 *Nat. Commun.* **10** 5641